

Final report

Mechanisms and role of acetylcholine signaling acting upon GnRH neurons of mice: a novel regulatory pathway of reproduction

Research laboratory: Laboratory of Endocrine Neurobiology, Institute of Experimental Medicine, Eötvös Loránd Research Network, Budapest
Project ID: **K 128278**
Start date: 01-12-2018
Closing date: 30-11-2022
PI: Zsolt Liposits

The hypothalamo-hypophyseal system is in charge of regulating reproduction centrally. At the hypothalamic level, the master neuropeptide, gonadotropin-releasing hormone (GnRH) has a pivotal role in orchestrating the downstream endocrine events. Failure in proper neuronal and hormonal signaling to the GnRH system results in malfunction of the hypothalamo-pituitary-gonadal (HPG) axis. Our recent efforts have delineated novel regulatory mechanisms exerted by estradiol, ghrelin, glucagon-like peptide -1 (GLP-1), secretin and kisspeptin. We have also discovered that retrograde endocannabinoid and nitric oxide (NO) signaling mechanisms are hired by the activated G-protein-coupled receptors. The retrograde messengers modify the activity of the most powerful neuronal regulators of GnRH neurons, the GABA- and glutamate-ergic presynaptic boutons. In the current grant period, we primarily have studied the regulatory role of acetylcholine signaling upon GnRH neurons and elucidated the structural, molecular and electrophysiological attributes of the interneuronal communication. The funding also contributed to success of further studies addressing other novel regulators of reproduction.

I. Outline of result parcellation and description

In this final report, we present results in three thematic groups (I-III).

I. Modulation of the GnRH neuronal system by acetylcholine signaling

The main goals of this project have been:

1. To explore the putative structural networking of central cholinergic and GnRH neuronal systems.
2. To reveal the types and subunits of functional acetylcholine receptors expressed in GnRH neurons.
3. To monitor the impact of nicotinic and muscarinic signaling on electrophysiological performance of GnRH neurons and shed light on the involved molecular mechanism/s.
4. To elucidate the *in vivo* effect of increased cholinergic tone upon luteinizing hormone (LH) secretion using pharmacogenetics.

II. Exploration of further novel, central regulators of reproduction

1. Impact of insulin-like growth factor 1 (IGF-1) upon electrophysiology of GnRH neurons
2. Effects of gonadal cycle on expression of genes coding for neuropeptide-, growth factor- and

orphan GPC-receptors.

III. Expanding the biological role of known regulatory peptides of the GnRH system

1. Ghrelin increases food intake via targeting the lateral parabrachial nucleus
2. Effects of orexin upon the mesolimbic and mesocortical dopamine projections

II. Summary of applied techniques

We applied a multidisciplinary approach exploiting modern structural and functional techniques as follows:

1. Animals

Wild-type and transgenic mice of both sexes. Wild type male rats.

2. Molecular methods

Quantitative, real-time PCR, Affimetrix microarray, pathway analysis, bioinformatics

3. Structural, neuroanatomical techniques

Immunocytochemistry, multiple-immunolabeling. Confocal laser microscopy. Transmission immune-electron microscopy. 3DISCO immunolabeling. Neuron network reconstruction. Laser capture microdissection. Quantitative analysis. Retrograde, viral, neuronal tract tracing.

4. Functional methods

Whole cell patch-clamp electrophysiology. Pharmacogenetics. Transgenic animals, hormone measurement by ELISA.

III. Summary of results

1. Modulation of the GnRH neuronal system by acetylcholine signaling

The publishing policy of our Institute has recently been changed favoring the dissemination of complete studies/results in Nature-indexed journals. To fulfill this requirement, we have not published yet any part of the complex study. The submission of the manuscript is scheduled for June 2023. Therefore, we present the achieved main results here in full details.

1. Exploration of networking between the central cholinergic and GnRH neuronal systems

Light microscopic correlates of networking

For structural evaluation and quantitative analysis of the putative interneuronal communication of the central cholinergic and the GnRH systems, double immunofluorescence labelling combined with 3DISCO method was used on paramedian sagittal slices of GnRH-GFP transgenic mouse brain that contained the distribution sites of GnRH neurons in the medial septum, the vertical limb of the diagonal band of Broca, the region of the organum vasculosum laminae terminalis, the medial preoptic area and the anterior hypothalamic area (**Fig. 1.**).

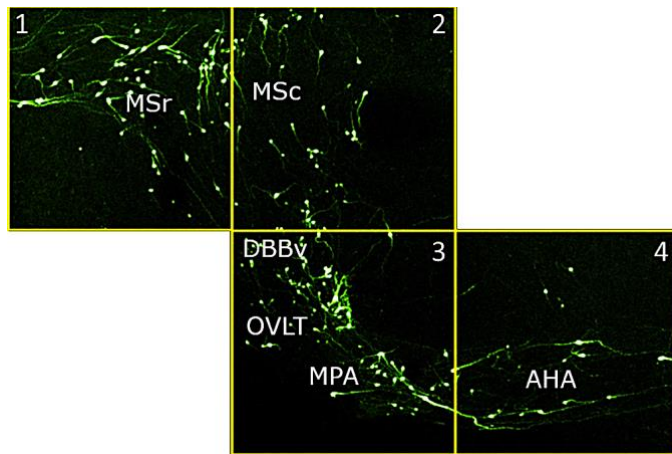


Fig. 1. Distribution of GnRH-GFP IR elements revealed by 3DISCO immunofluorescent microscopy. Adjacent frames (yellow squares, numbered from 1 to 4) represent the scanning areas of image acquisition via confocal microscopy in 1 mm thick, brain slice cut in the paramedian sagittal plane. The frames include the following neuroanatomical structures: **1.** Medial septum, rostral part (MSr); **2.** Medial septum, caudal part (MSc); **3.** Diagonal band of Broca, vertical part (DBBV), organum vasculosum of the lamina terminalis (OVLT) and medial preoptic area (MPA); **4.** Anterior hypothalamic area (AHA).

The cholinergic axons were identified by their vesicular acetylcholine transporter (VACHT) content, while GnRH-immunoreactive (IR) profiles were visualized by immunostaining of the expressed green fluorescent protein (GFP). GnRH neurons were found in overlap with VACHT-IR axons distributed in the sampled regions (**Figs. 2a, b**). Altogether, 4,899 optical slices (mean \pm SEM: 816 \pm 64 per brain) were evaluated. In each optical slice, the number of VACHT-IR axons juxtaposed to GnRH-IR perikarya, and dendrites was determined. Juxtapositions were justified with high precision in orthogonal view layout. Many VACHT-IR axon varicosities (1040 \pm 96 SEM, n = 6) were identified in juxtaposition with GnRH-IR profiles (**Figs. 2c, d**). Most of them (86.5 \pm 3.2 percent,) terminated on GnRH dendrites (**Fig. 2c, e**) and only a smaller fraction (13.5 \pm 3.2 percent) contacted GnRH perikarya (909 \pm 100.12 dendritic vs 131 \pm 23.68 somatic input, n = 6; *t*-test, p = 1.928E-05; **Fig. 2d**). In these samples, as an average, 37.4 \pm 5.1 percent of reconstructed GnRH-IR perikarya (186 \pm 20) received cholinergic inputs (68 \pm 9.66 innervated vs 118 \pm 16.9 non-innervated GnRH-IR perikarya, n = 6; *t*-test, p = 0.029, **Fig. 2f**).

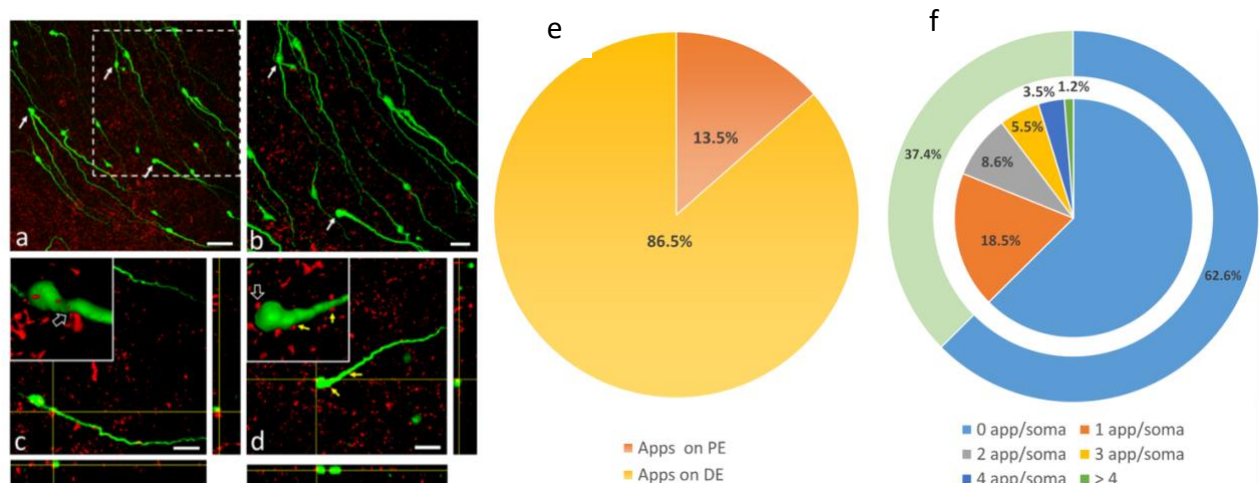


Fig. 2. GnRH neurons receive cholinergic inputs as revealed by double immunostaining and 3DISCO method. **a.** A stack of confocal image planes projected in the z direction represents numerous GnRH neurons (green channel, arrows) and VACHT-immunoreactive (IR) axon varicosities (red channel). **b.** A part of the image stack shown by dashed square in **Fig. 2a** was reconstructed as a 3D surface model using ImageJ/Fiji software. Note the overlap of the two immunolabeled systems. **c.** Axo-dendritic contact between a VACHT-IR axon and a GnRH neuron is shown in both 3D surface model (inset, arrow) and orthogonal views of stacks

(yellow crosshairs). **d.** The inset demonstrates an axo-somatic juxtaposition (empty arrow) in 3D image. The same communication site is confirmed in orthogonal views (yellow crosshairs). Two other cholinergic axon varicosities (yellow arrows) juxtaposed to the same GnRH neuron indicate the existence of multiple contact sites. **e.** The cholinergic axons predominantly communicate with GnRH dendrites (86.5%), the perikarya are less frequently targeted (13.5%). Apps on PE: appositions on perikarya, Apps on DE: appositions on dendrites. **f.** About one third (37,4 %) of the analyzed the GnRH perikarya received VAcHT-IR inputs. The inner pie diagram depicts the percentage distribution of VAcHT-IR axon beads juxtaposed to the same GnRH perikaryon. App/soma: apposition per soma. Scale bars: a: 50 μ m; b: 25 μ m; c and d: 20 μ m.

2. Ultrastructural correlates of networking

The networking among VAcHT-IR axons and GnRH neurons was also confirmed at the ultrastructural level using pre-embedding double immunocytochemistry. For labelling of VAcHT-IR axons nickel-3,3 diaminobenzidine (Ni-DAB) chromogen was used (**Figs. 3a, b**), while the GnRH immunoreactive profiles were visualized by silver-intensified colloidal gold particles (**Figs. 3c, d**). In the residence area of hypophysiotropic GnRH neurons, the medial septum-diagonal band of Broca-OVLT continuum, VAcHT-expressing axons appeared in juxtaposition to cell bodies and dendrites (**Fig. 3a**) and formed synapses (**Fig. 3b**). Based upon the different physico-chemical properties of the used chromogens, the GnRH and VAcHT-IR profiles were clearly distinguishable from each other even at low power electron microscopic screening (**Fig. 3d**). The juxtaposition of cholinergic axon beads to dendritic and somatic domains of GnRH neurons without glial process interposition was confirmed at the ultrastructural level. Tracing the juxtaposed profiles through series of ultrathin sections revealed the synaptic engagement of VAcHT-IR, cholinergic axons with dendrites (**Fig. 3e**) and perikarya (**Figs. 3f, g**) of GnRH neurons suggesting a direct regulatory influence of the cholinergic system upon the GnRH neuron assembly.

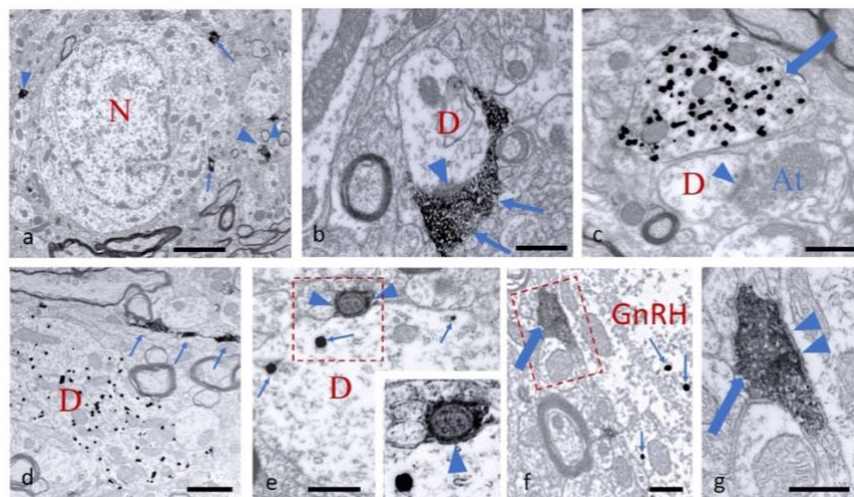


Fig. 3. Ultrastructural detection of cholinergic axons and GnRH-immunoreactive (IR) profiles in the medial preoptic area (mPOA) of mouse. **a.** Vesicular acetylcholine transporter (VAcHT)-containing axons labelled by Ni-DAB chromogen are distributed in the neuropil of the mPOA contacting cell bodies (arrows) and dendrites (arrowheads). A non-labelled neuron (N) is in the center of micrograph. **b.** A Ni-DAB chromogen-labelled cholinergic axon (arrows) synapses (arrowhead) on a cross-sectioned dendrite (D). **c.** Appearance of a cross-sectioned GnRH dendrite (arrow) filled with silver-intensified, colloidal gold particles. A nearby unlabeled dendrite (D) receives a synapsing (arrowhead) axon terminal (At). **d.** Simultaneous detection of a longitudinally sectioned GnRH dendrite (D) identified by silver coated-colloidal gold particles and a varicose, longitudinally cut VAcHT-IR axon (arrows) labelled by Ni-DAB chromogen.

e. Cross-sectioned GnRH-IR dendrite (D) communicating with a small sized cholinergic axon (arrowheads). Arrows point to the metallic label of the GnRH profile. The enframed region is shown at higher power in the inset, the arrowhead points to the postsynaptic membrane. *f.* Detail from a GnRH perikaryon (GnRH) that receives a cholinergic axon (thick arrow). Intensified, colloidal gold particles are indicated by small arrows. The communication site is enframed. *g.* High power view of the enframed area in **Fig. f**. The labelled, cholinergic axon (thick arrow) filled with small-sized synaptic vesicles establishes communication (arrowheads) with the GnRH perikaryon. Scale bars: **a**: 2 μ m; **d**: 1 μ m; **b** and **c**: 500 nm; **e-g**: 250 nm.

2. Characterization of acetylcholine receptors expressed in GnRH neurons

Expression of nicotinic and muscarinic acetylcholine receptors in hypophysiotropic GnRH neurons

Cytoplasmic samples (n = 70) were collected from GnRH-GFP neurons by patch pipette aspiration, sorted into separate cytoplasmic sample pools (CPs, n = 7) and examined by quantitative real time PCR (qRT-PCR). The primer probe sets used for detection of expression of genes coding for muscarinic and nicotinic receptors and housekeeping genes (*Hprt*, *Gapdh*) and GnRH Examination of the sample groups revealed the relative expression of the following nicotinic receptor subunits in GnRH neurons (mean \pm SE) (**Fig. 4b**): alpha 3 subunit (*Chrna3*) 0.026 ± 0.006 (2 of 7 CPs), alpha 4 subunit (*Chrna4*) 0.016 ± 0.009 (2 of 7 CPs), alpha 7 subunit (*Chrna7*) 0.018 ± 0.009 (3 of 7 CPs), beta 2 subunit (*Chrb2*) 0.015 ± 0.005 (4 of 7 CPs); beta 3 subunit (*Chrb3*) 0.023 ± 0.11 (4 of 7 CPs) and beta 4 subunit (*Chrb4*) 0.047 ± 0.016 (5-of 7 CPs). Regarding muscarinic receptors (m1-m5), muscarinic type 1 (*Chrm1*) 0.034 ± 0.004 (5 of 7 CPs), muscarinic type 2 (*Chrm2*) 0.011 ± 0.006 (2 of 7 samples), type 3 (*Chrm3*) 0.048 ± 0.016 (5 of 7 CPs), type 4 (*Chrm4*) 0.038 ± 0.013 (4 of 7 CPs) and type 5 (*Chrm5*) 0.037 ± 0.024 (3 of 7 CPs) receptor genes were also measured in the samples (**Fig. 4b.**) The expression of *Gnrh* gene (30.2 ± 4.68) was confirmed in all samples (**Fig. 4a**).

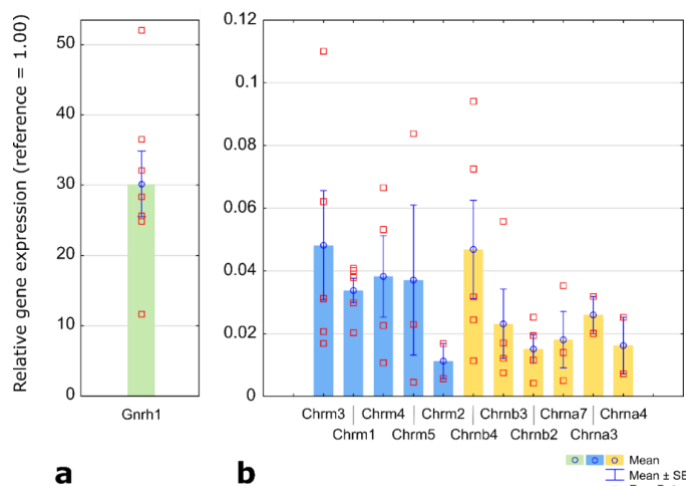


Fig. 4. Relative expression of *Gnrh1* gene (a) and various nicotinic and muscarinic acetylcholine receptor genes (b) in cytoplasmic sample pools of GnRH neurons revealed by qRT-PCR. The mean \pm standard error of raw gene expression data is shown for each subunit as a proportion of the mean of the two reference genes.

3. Effects of acetylcholine receptor activation on electrophysiology and signal transduction mechanisms of GnRH neurons

Cholinergic drugs modify the electrophysiological properties of GnRH neurons in acute brain slice preparation

1. Effects on firing

To evaluate effect of acetylcholine (ACh) on the electric activity of GnRH neurons, firing was recorded in whole-cell current clamp mode. Single bolus of ACh (100 μ M, shown by arrow in the recording), the natural ligand of the cholinergic system, evoked a biphasic change in the firing rate (**Fig. 5a**). First, it was elevated (stimulatory phase) then a subsequent robust inhibition (inhibitory phase) was observed. Thorough examination of the recording, however, revealed that the stimulatory phase could be further divided into two sub-phases (phase I.=0.5min, phase II.=3 min), while no subdivisions could be defined in the inhibitory phase (phase III.=3 min). All the three phases represented significant change in the firing rate (**Fig. 5a**, phase I.: $409.3 \pm 49.44\%$, phase II.: $285.3 \pm 39.91\%$, phase III.: $44.6 \pm 8.93\%$, washout: $98.7 \pm 10.18\%$ of the control firing rate). Frequency distribution of firing rate is shown under the recording. The horizontal, colored lines under the recording represent the various phases, matching to the color of the bar graph.

In addition to ACh, we applied carbachol (40 μ M) in a single bolus, another ligand of the ACh-R, which cannot be eliminated by the esterase activity of the brain slice. Administration of carbachol (shown by arrow in the recording) also triggered a biphasic action in the firing rate (**Fig. 5b**), demonstrating a stimulatory phase and a subsequent inhibitory phase. Furthermore, the stimulatory phase could be divided into two sub-phases, revealing three phases eventually (phases I-II-III.) like the ones observed in the case of ACh. The three phases also showed significant change in the firing rate (**Fig. 5b**, phase I.: $186.9 \pm 20.47\%$, phase II.: $140.4 \pm 9.23\%$, phase III.: $28.6 \pm 7.486\%$, washout: $105.1 \pm 6.27\%$ of the control firing rate). Frequency distribution of firing rate is shown under the recording. The horizontal, colored lines under the recording represent the various phases, matching to the colors of the bar graph.

To determine which receptors, play role in the observed effect, the brain slices were pre-treated with mecamylamine (10 μ M, horizontal black line above the recording), the nicotinic ACh-R (nACh-R) antagonist, and then carbachol was applied. Carbachol application first stimulated firing activity of GnRH neurons, which was followed by an inhibition (**Fig. 5c**). Examination of the recordings, however, clearly showed that phase I. was absent whereas phase II. was present in the stimulatory phase, indicating that a functional nicotinic ACh-R is responsible for phase I. Statistical analysis revealed that phase II. and phase III. represent significant changes in the firing rate (**Fig. 5c**, phase I.: $99.4 \pm 3.311\%$, phase II.: $156.9 \pm 12.16\%$, phase III.: $37.7 \pm 7.67\%$, washout: $103.4 \pm 5.29\%$ of the control firing rate), suggesting that muscarinic ACh-Rs also function in GnRH neurons. Frequency distribution of firing rate is shown under the recording.

To reveal role of muscarinic ACh-Rs (mACh-R) in GnRH neurons, the brain slices were pre-treated with atropine (10 μ M, horizontal black line above the recording), the muscarinic ACh-R antagonist, and then carbachol was added in a single bolus to the aCSF in the measuring chamber. The measurement demonstrated that carbachol induced a short stimulatory phase, but no inhibition occurred (**Fig. 5d**). The short stimulation resembled to phase I. In contrast, phases II. and III. were absent (**Fig. 5d**, phase I.: $179.3 \pm 12.6\%$, phase II.: $104.5 \pm 4.95\%$, phase III.: $94.9 \pm 6.485\%$, washout: $102.9 \pm 3.912\%$ of the control firing rate), showing functional presence of mACh-Rs.

All together, these results indicated that phase I. represents activation of nACh-Rs, phase II. represents stimulation via various mACh-Rs, and phase III. represents inhibition via other mACh-R subtypes.

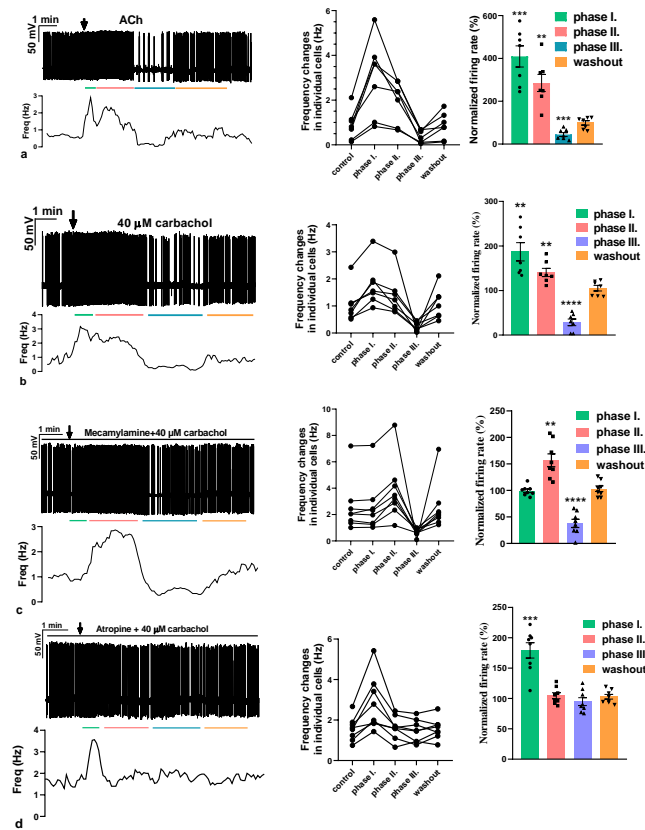


Fig. 5. Representative recordings show the effect of acetylcholine (ACh, 50 μ M) or carbachol on the firing rate of GnRH neurons in male mice. a. ACh evoked a biphasic action, first it increased firing rate then a robust inhibition occurred. **b.** Carbachol (40 μ M) also triggered a biphasic effect with an initial elevation followed by a subsequent decrease in the firing rate. **c.** Mecamylamine (10 μ M) pre-treatment eliminated the first, 0.5 min part of the elevation phase suggesting that the facilitatory phase can be further divided into two subphases representing nicotinic (phase I) and muscarinic (phase II) stimulatory actions, respectively. **d.** Atropine (10 μ M) pre-treatment abolished both phase II of the facilitation and the inhibitory phase (phase III) demonstrating that these phases represent muscarinic effects.

Arrow shows the time of administration of ACh or carbachol. Horizontal black line above the recordings represents application of inhibitors (nicotinic ACh receptor blocker mecamylamine or muscarinic ACh receptor blocker atropine). Changes in the firing rate of individual GnRH neurons and the percentage changes are shown besides each recording. Frequency distribution of firing rate is graphed under each recording. Phase I=0.5 min, phase II=3 min, phase III=3 min. The colored lines under the recordings match the colors of the bar graphs and represent the various phases. **= $p < 0.01$, ***= $p < 0.005$, ****= $p < 0.001$.

Effects on ion current and mPSCs

Our results regarding firing rate data indicated functional presence of both nACh-R and mACh-R in GnRH neurons. Next, we studied effect of activation of these receptors on the membrane current and mPSCs in voltage-clamp mode at -70 mV. Application of carbachol in a single bolus triggered a transient fast inward current (amplitude = -36.9 ± 3.09 pA, Student's t-test: N/n=3/9, $p=0.0001$, $t=11.95$, $df=8$; duration = 47.9 ± 12.34 s) (**Fig. 6a**). Recordings also showed that frequency of mPSCs significantly decreased (65.7 ± 6.01 % of the control value, **Fig. 6a**). The zoomed figures

and the graph next to the recording and the frequency distribution Fig. below the recording also demonstrate this observation.

We hypothesized that activation of nACh-R was responsible for the inward current. Therefore, the brain slice was pre-treated with mecamylamine (10 μM , horizontal black line above the recording), and then carbachol was added to the aCSF (**Fig. 6b**). Absence of the inward current confirmed the hypothesis that activation of nACh-R evoked the change in the membrane current. Nevertheless, the zoomed figures and the graphs next to the recording clearly demonstrated that the significant decrease in the frequency of the mPSCs was still observable ($57.2 \pm 6.88\%$ of the control value, **Fig. 6b**). The frequency distribution graph below the recording confirmed this observation.

The results above suggested that mACh-Rs play role in the frequency change of the mPSCs. Thus, the slices were pre-treated with a cocktail of mecamylamine+atropine (10-10 μM , horizontal black line above the recording), and then carbachol was added to the aCSF (**Fig. 6c**). before administration of carbachol. The recordings and the graphs demonstrated that neither inward current nor decrease in the frequency of mPSCs were detected under these circumstances (frequency: $97.2 \pm 3.41\%$ of the control value, **Fig. 6c**).

To confirm role of mACh-Rs further in the decrease in the frequency of mPSCs, muscarine (100 μM) was added to the aCSF in a single bolus. The measurement revealed that no inward current was evoked by muscarine. Nevertheless, a significant decrease in the frequency of mPSCs was detected ($68.1 \pm 6.67\%$ of the control value, **Fig. 6d**). However, atropine pre-treatment abolished this change in the frequency ($103.5 \pm 5.11\%$ of the control value, **Fig. 6e**). These results regarding the frequency changes are summarized in the bar graph (**Fig. 6f**) showing that mAChRs play role in the decrease of frequency of mPSCs.

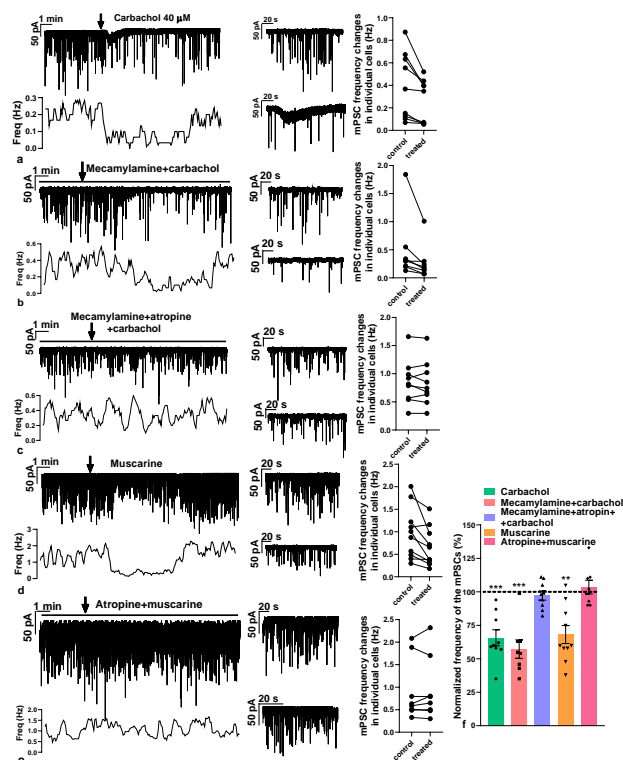


Fig. 6. Representative recordings demonstrate that the ACh agonist carbachol (40 μM) evokes an inward current and then an inhibitory action on mPSCs of GnRH neurons in the presence of tetrodotoxin (660 nM) representing involvement of both nicotinic and inhibitory muscarinic receptor subtypes. **a.** Carbachol triggers a fast inward current and a slower inhibitory effect in the frequency of mPSCs. **b.** Mecamylamine (nicotinic ACh-R antagonist) pre-treatment (10 μM) reveals that the fast action is related to nicotinic

receptor subtypes. **c.** Simultaneous pre-treatment with mecamylamine and atropine (muscarinic AChR antagonist, 10 μ M) eliminates both the inward current and the inhibitory effect of carbachol. **d.** Muscarine (100 μ M) evokes exclusively the inhibitory action in mPSCs. **e.** This inhibitory effect is abolished by atropine pre-treatment. **f.** The bar graph summarizes the results detailed above. **= $p < 0.01$, ***= $p < 0.005$. Horizontal black lines above the recordings show presence of various AChR receptor subtype inhibitors (mecamylamine, atropine) in the aCSF. Arrow shows the time of administration of carbachol or muscarine. Zoomed 2.5 min recordings of control (upper graph) and treated (lower graph) regions are besides the recordings. Changes in the frequency of mPSCs of individual GnRH neurons are shown besides these zoomed recordings. Frequency distribution of the mPSCs is graphed under each recording.

Electrophysiological characterization of functional nicotinic receptor subtypes involved in control of GnRH

Our present results clearly demonstrated that functional nACh-Rs play role in evoking the inward current observed upon administration of carbachol. These receptors consist of various subunits; therefore, we investigated presence of these elements in the membrane of GnRH neurons using whole-cell voltage clamp measurements. Application of nicotine (10 μ M, broadband agonist of nACh-Rs) triggered a robust inward current (amplitude = -41.5 ± 9.05 pA, duration = 58.9 ± 18.3 s, **Fig. 7a, d**). Then the slice was pre-treated with DHBE (1 μ M, antagonist of the $\alpha 4\beta 2$ subunit) and nicotine was applied again to the same neuron. An inward current was evoked again, however, its amplitude was significantly lower comparing to the one observed when nicotine was added alone (amplitude = -18.4 ± 3.41 pA, duration = 84.4 ± 33.41 s, **Fig. 7b, d**) showing, that $\alpha 4\beta 2$ subunits play role in the observed effect. Next, α -conotoxin AuIB (1 μ M, antagonist of $\alpha 3\beta 4$ subunit) was added to the aCSF containing DHBE and nicotine was administered again to the same neuron. This inhibitor cocktail significantly decreased the amplitude further (amplitude = -9.2 ± 2.36 pA, duration = 78.2 ± 38.6 s, **Fig. 7c, d**), but did not eliminate it completely. These results suggest that a GnRH neuron expressing $\alpha 4\beta 2$ subunit also present $\alpha 3\beta 4$ subunit. Nevertheless, the antagonist cocktail did not abolish the evoked inward current completely, indicating that a further nACh-R subunit also exists in GnRH neurons.

Thus, our present results revealed that if $\alpha 4\beta 2$ subunit is present, then $\alpha 3\beta 4$ subunit is also expressed in GnRH neurons. Next, we investigated the reverse order question: if a GnRH neuron expresses $\alpha 3\beta 4$ subunit then it also present $\alpha 4\beta 2$? Therefore, after measuring the nicotine-evoked inward current (amplitude = -42.9 ± 7.89 pA, duration = 68.7 ± 21.3 s, **Fig. 7e, h**), then α -conotoxin AuIB was first added to the aCSF, and the nicotinic response was recorded again in the same neuron. Conotoxin pre-treatment significantly decreased amplitude of the inward current but not eliminated (amplitude = -19.2 ± 2.83 pA, duration = 74.1 ± 28.39 s, **Fig. 7f, h**) showing functional presence of the $\alpha 3\beta 4$ subunits. Then DHBE was also added to the aCSF. This cocktail significantly lowered the amplitude further but not abolished it (amplitude = -9.2 ± 1.74 pA, duration = 71.1 ± 26.98 s, **Fig. 7g, h**).

To present further evidence that $\alpha 4\beta 2$ subunits are expressed in GnRH neurons, RJR2403 (100 μ M, selective agonist of the $\alpha 4\beta 2$ subunits) was applied in a single bolus. Application of RJR evoked an inward current (amplitude = -22.9 ± 4.15 pA, duration = 98.9 ± 38.15 s, **Fig. 7i, l**), which was abolished completely by DHBE pre-treatment (amplitude = -1.2 ± 1.23 pA, **Fig. 7j, l**).

Our results indicated that beside $\alpha 4\beta 2$ and $\alpha 3\beta 4$ further subunits were present in GnRH neurons. We hypothesized from the mRNA data that $\alpha 7$ subunit was also expressed. Therefore, PNU282987 (100 μ M, selective agonist of the $\alpha 7$ subunits) was applied into the aCSF in a single bolus. It evoked a low amplitude but still significant inward current (amplitude = -11.2 ± 1.88 pA, duration = $88.6 \pm$

25.15 s, **Fig. 7k, l**), resembling the ones seen in Fig. 7c and g, suggesting that $\alpha 7$ subunits also function in GnRH neurons.

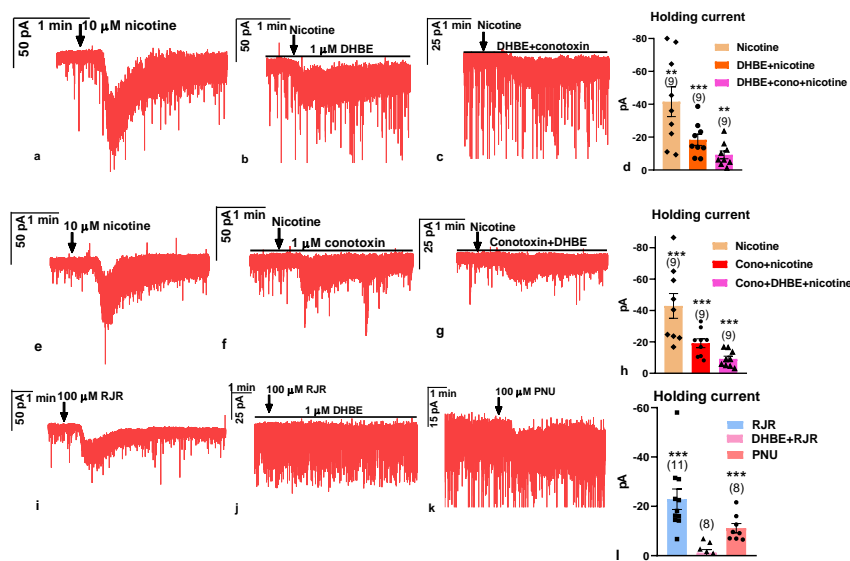


Fig.7. Representative whole-cell patch voltage clamp recordings demonstrate that nicotine evoked an inward current in GnRH neurons, depending on the subunit composition of the ionotropic AChR. a. Nicotine administration (10 μM) induced a robust inward current. **b.** The $\alpha 4\beta 2$ nAChR antagonist, DHBE (1 μM) significantly reduced the nicotine-evoked inward current measured in the same neuron as in “**Fig. a**”. **c.** The co-application of $\alpha 3\beta 4$ antagonist, conotoxin (1 μM) with DHBE dampened the nicotine-evoked inward current further but did not eliminate it. The recording was carried out in the same neuron as in “**Figs. a and b**” demonstrating that neurons expressing $\alpha 4\beta 2$ receptor also present $\alpha 3\beta 4$ receptor in their membrane. **d.** The bar graph summarizes the significant inward currents measured. **e)** In another neuron, nicotine also induced a strong inward current. **f.** The $\alpha 3\beta 4$ receptor antagonist, conotoxin (1 μM) significantly reduced the evoked inward current measured in the same neuron as in “**Fig. e**”. **g.** Co-administration of DHBE attenuated the inward current further but did not abolish it. The recording was measured in the same neuron as in “**Figs. e and f**” showing that neurons expressing the $\alpha 3\beta 4$ receptor also contain functional $\alpha 4\beta 2$ receptor in their membrane. **h.** The bar graph summarizes these results. **i-j.** The $\alpha 4\beta 2$ agonist, RJR (100 μM) also triggered an inward current, which was abolished by DHBE pre-treatment. **k.** The $\alpha 7$ nAChR agonist, PNU (100 μM) also evoked a low-amplitude inward current. **l.** The bar graph summarizes these results. DHBE= dihydro- β -erythroidine ($\alpha 4\beta 2$ antagonist), conotoxin= α -conotoxin AuIB ($\alpha 3\beta 4$ antagonist), RJR=RJR2403 ($\alpha 4\beta 2$ agonist), PNU=282987 ($\alpha 7$ agonist). Arrow shows administration of various agonists. *= $p < 0.05$, **= $p < 0.01$, ***= $p < 0.005$

Electrophysiological characterization of functional muscarinic receptors in modulation of GnRH neuron activity

Effects on firing

Our present results indicated that beside the nACh-Rs functional mACh-R subtypes also exist in GnRH neurons. Therefore, function of these various subtypes was examined by measuring firing activity in GnRH neurons using whole-cell current clamp method. Muscarine (100 μM , broad-band agonist of mACh-Rs) was administered in a single bolus. It evoked a biphasic action. In the first 3 min period (phase I., represented by a horizontal orange line under the recording) muscarine elevated firing rate significantly (147.6 ± 10.28 % of the control firing rate, **Fig. 8a**). In the second 3 min period (phase II., represented by a horizontal blue line) an obvious significant decrease was observed in the firing rate (54.5 ± 6.9 % of the control firing rate, **Fig. 8a**). Two subtypes of mACh-

R are stimulatory (m1 and m3) whereas two other subtypes are inhibitory (m2 and m4). First, we examined function of m4 by pre-treating the brain slices with tropicamide (2 μ M, selective inhibitor of the m4 subtype of mACh-Rs, represented by a black horizontal line above the recording) then muscarine was administered. The recording clearly shows that both the stimulatory and the inhibitory phases exist (**Fig. 8b**). Firing rate significantly increased up to 152 ± 14.8 % of the control firing rate and then significantly decreased to the 78.3 ± 5.53 % of the control value. However, phase II. represented a decrease that was milder than without tropicamide, suggesting that beside m4 another inhibitory subtype is expressed.

Thus, m2, the other inhibitory mACh-R subtype was blocked by adding methoctramine (2 μ M, selective inhibitor of the m2 subtype of mACh-Rs, represented by a black horizontal line above the recording) then muscarine was applied. The stimulatory phase I. still existed in the presence of methoctramine revealing a significant increase in the firing rate (145.6 ± 6.59 % of the control value, **Fig. 8c**). The inhibitory phase II. also existed because firing rate significantly diminished (80.8 ± 3.45 % of the control value, **Fig. 8c**). The phase II., however, displayed a smaller decrease than in the absence of the m2 or m4 antagonists, revealing role of the m2 subtype.

Next, we antagonized both inhibitory subtypes. In the presence of a cocktail of tropicamide and methoctramine, the stimulatory phase I. existed (150.8 ± 12.61 % of the control firing rate), but no inhibitory phase II. could be seen, rather a stimulation was observed in the phase II. period (122.4 ± 8.76 % of the control value) (**Fig. 8d**). The changes in both phases were significant. The stimulatory period, therefore, lasted much longer in the presence of the m2-m4 antagonists.

We also studied function of the stimulatory mACh-R subtypes m1 and m3. First pirenzepine (1 μ M, selective antagonist of the m1 subtype of mACh-Rs) was added to the cocktail of tropicamide and methoctramine and then muscarine was applied. In the presence of these three antagonists, muscarine significantly increased firing rate in phase I. (118.9 ± 4.5 % of the control firing rate, **Fig. 8e**). Nevertheless, this value of the increase was lower than without pirenzepine, showing role of m1 in the stimulation. Phase II., however, presented no significant change at all (102.4 ± 6.42 % of the control value). Thus, duration of the stimulation was not longer than three minutes.

Role of m3, the other stimulatory mACh-R subtype was also investigated. Darifenacin (1 μ M, selective antagonist of the m3 subtype of mACh-Rs) was added to the cocktail of tropicamide and methoctramine and then muscarine was applied. Phase I. presented a significant elevation in the firing rate (119.4 ± 4.18 % of the control firing rate, **Fig. 8f**). Phase II. also displayed a significant increase in the firing rate (124.0 ± 9.71 % of the control value, **Fig. 8f**, thus the stimulation lasted much longer than three minutes.

Finally, effect of muscarine was examined in the presence of m1-m2-m3-m4 antagonists. This cocktail abolished both phase I. (105.3 ± 8.31 % of the control value) and phase II. (103.2 ± 7.89 % of the control firing rate) completely (**Fig. 8g**).

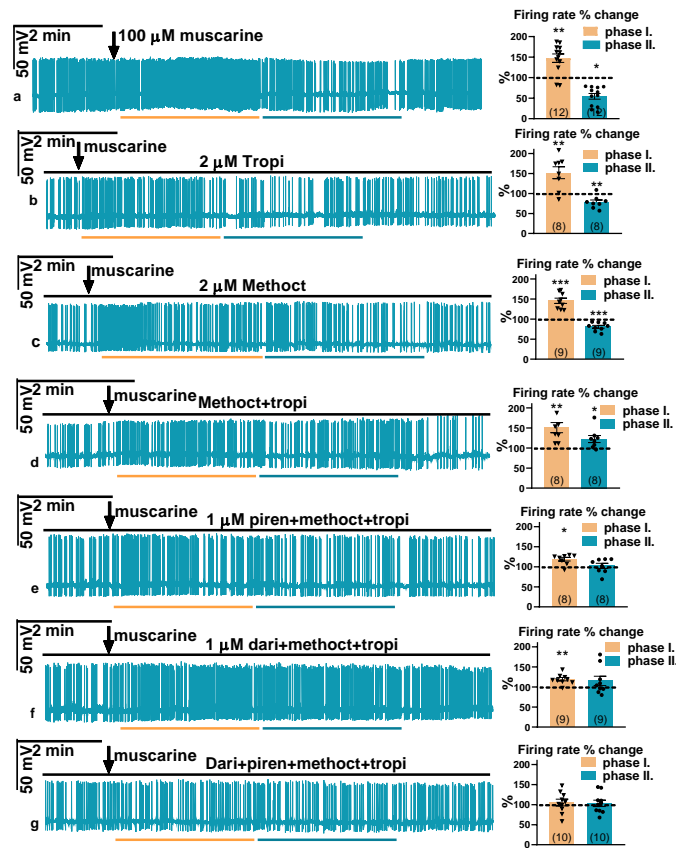


Fig. 8. Representative whole-cell patch current-clamp recordings demonstrate that muscarine evoked a biphasic effect on firing of GnRH neurons expressing various muscarine receptor subtypes. *a.* In the first, approximately 2.5-minute period, muscarine (100 μ M) enhanced (phase I) the firing rate of GnRH neuron followed by a decreased activity period (phase II). *b.* The inhibitory, m4-muscarine receptor antagonist tropicamide (2 μ M) dampened the inhibitory effect of muscarine (as seen in phase II.). *c.* The inhibitory m2-muscarine receptor antagonist, methoctramine (2 μ M) also decreased the inhibitory effect of muscarine (phase II.). *d.* Co-administration of tropicamide and methoctramine eliminated the inhibitory action of muscarine (phase II.). *e.* The stimulatory, m1-muscarine receptor antagonist, pirenzepine (1 μ M) dampened the stimulatory effect of muscarine (as seen in phase I.) in the presence of the m2-m4 antagonists. *f.* The stimulatory, m3-muscarine receptor antagonist, darifenacin (1 μ M) also attenuated the stimulatory effect of muscarine (phase I.). *g.* Neither facilitation nor inhibition was observed when a cocktail of all four antagonists is present in the aCSF. Black line above each recording shows presence of cocktails of various muscarine receptor subtype inhibitors in the aCSF (dari=darifenacin, methoct=methoctramine, piren=pirenzepine, tropi=tropicamide). Light brown line under each recording presents period of stimulatory phase (phase I.) and blue line represents that of the inhibitory phase (phase II.). Arrows show administration of muscarine. *= $p < 0.05$, **= $p < 0.01$, ***= $p < 0.005$.

Effects on mPSCs and involved mechanisms

To examine the signaling pathways involved the ACh-evoked firing rate changes and roles of inhibitory/stimulatory muscarinic receptors, mPSCs were investigated using whole-cell patch clamp measurements with voltage clamp method. First, blockade of the inhibitory receptors was carried out with a cocktail of tropicamide and methoctramine, inhibitors of the m2 and m4 muscarinic receptors, respectively, after a 1-min-long control period. The treatment resulted in a significant

elevation in the frequency of the mPSCs suggesting a tonic release of ACh ($127.3 \pm 8.50\%$ of the control value, **Figs. 9. a, e**). Then muscarine ($100 \mu\text{M}$) was added in a single bolus into the measuring chamber in the continuous presence of the blocker cocktail. Muscarine significantly increased the frequency further ($139.1 \pm 14.75\%$ of the value just before adding muscarine, **Figs. 9. a, f**). In the second round, the m1 and m3 stimulatory receptors were antagonized with a cocktail of darifenacin and pirenzepine and the measurements were carried out again. Blockade of the stimulatory receptors decreased frequency of the mPSCs significantly, confirming the tonic release of ACh ($80.7 \pm 2.67\%$ of the control value, **Figs. 9. b, e**). Muscarine administration diminished the frequency significantly further ($139.1 \pm 14.75\%$ of the value just before adding muscarine, **Figs. 9. b, f**).

Our earlier studies revealed that activation of retrograde 2-AG endocannabinoid signaling pathways can both increase and decrease frequency of mPSCs in GnRH neurons. Therefore, THL, an inhibitor of the 2-AG endocannabinoid production, was applied intracellularly in the intracellular patch pipette solution. Under this condition, cocktail of tropicamide + methocitramine evoked no significant change in the frequency of the mPSCs ($102.2 \pm 4.1\%$ of the control value, **Figs. 9. c, e**), and muscarine application triggered no significant change either ($106.5 \pm 4.17\%$ of the control value, **Figs. 9. c, f**). Similarly, cocktail of darifenacin + pirenzepine resulted in no significant change in the frequency in the intracellular presence of THL ($102.3 \pm 5.1\%$ of the control value, **Fig. 9. d, e**), and muscarine induced no significant alteration of the frequency either ($106.4 \pm 4.97\%$ of the control value, **Figs. 9. d, f**). These data reveal role of the retrograde endocannabinoid signaling pathways in the muscarinic signalization of GnRH neurons.

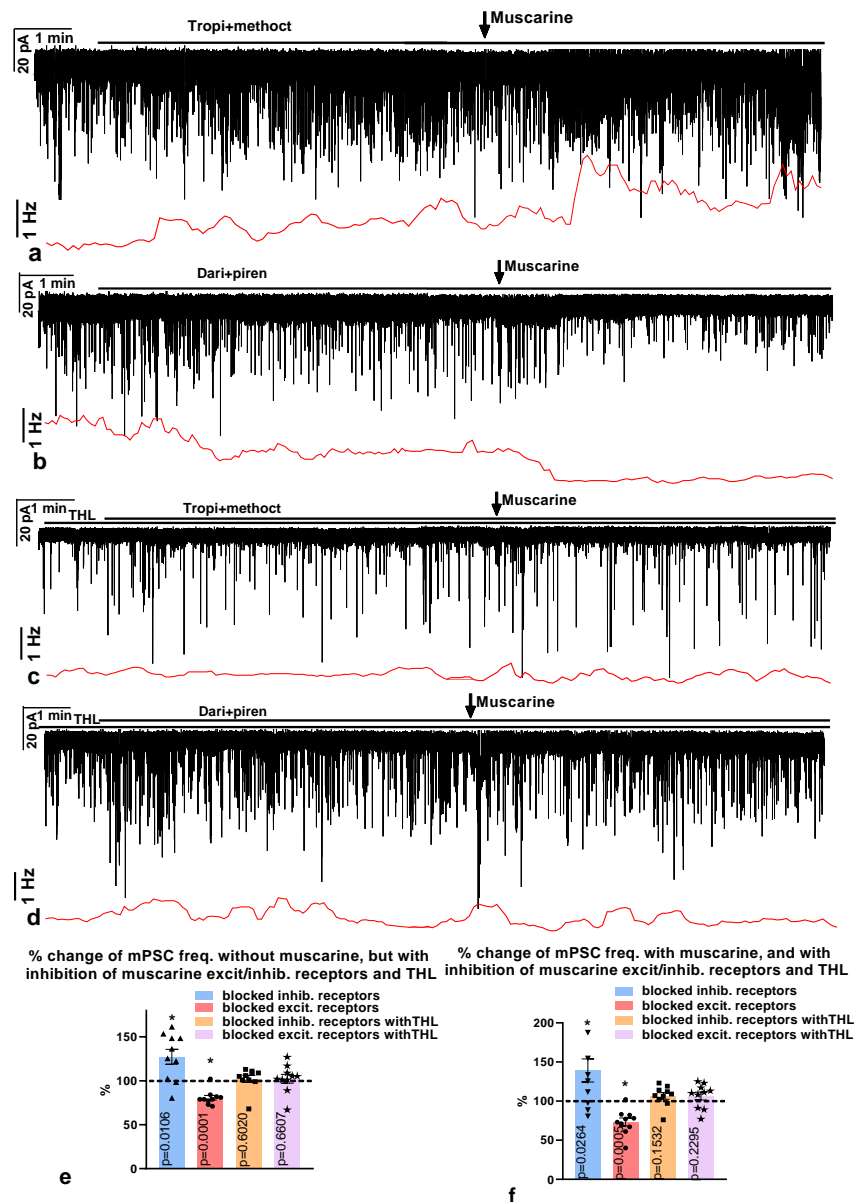


Fig. 9. Representative recordings demonstrate effect of blockade of inhibitory (tropicamide + methoctramine) or stimulatory (darifenacin + pirenzepine) muscarinic receptors and muscarine on mPSCs in GnRH neurons in the intracellular absence/presence of THL, an inhibitor of retrograde 2-AG endocannabinoid signaling pathway. **a.** Blockade of inhibitory receptors increased frequency of mPSCs. Application of muscarine elevated the frequency further. **b.** In contrast, blockade of stimulatory receptors diminished frequency of mPSCs, and muscarine reduced it further. **c-d.** Intracellular presence of THL, however, abolished the effects, neither blockade of inhibitory/stimulatory receptors, nor application of muscarine evoked any significant action on the frequency. **e-f.** The bar graphs summarize these significant actions. Horizontal black lines above the recordings show presence of various inhibitors (THL, dari=darifenacin, methoct=methoctramine, piren=pirenzepine, tropi=tropicamide) and arrow points time of muscarine administration. * = $p < 0.05$. Frequency distribution graphs are located under each recording.

4. Impact of pharmacogenetic activation of the central cholinergic system upon secretion of luteinizing hormone (LH)

Pharmacogenetic approach was used to study *in vivo* the effect of increased cholinergic tone upon the secretion of luteinizing hormone (LH) which precisely parallels the discharge of GnRH onto the portal circulation. To achieve this goal a transgenic mice line was established (*Chat-Gq (hM3Dq) DREADD*) that expressed the DREADD receptor exclusively in central cholinergic neurons (**Fig 10**)

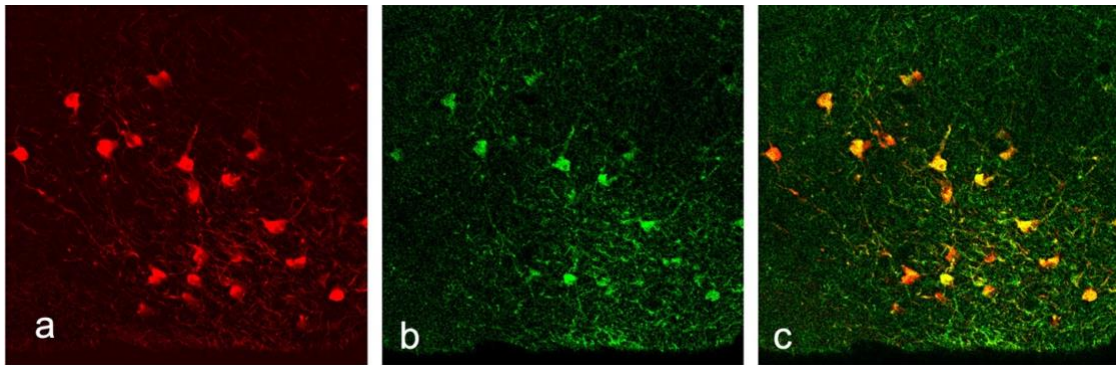


Fig. 10. Expression of *Gq (hM3Dq) DREADD* receptor in cholinergic neurons of the basal forebrain in the *Chat-Gq (hM3Dq) DREADD* mouse. **a.** Cholinergic neurons (red) immunolabelled for the marker enzyme, choline acetyltransferase. **b.** The same cholinergic neuron cluster shown in **a** is immunopositive for citrine (green), the reporter protein identifying the expression sites of the DREADD receptor. Note the intense labelling of both perikarya and neuronal processes. **c.** Merged image of **a** and **b** demonstrates the total overlap of *Chat* and citrine immunoreactivities. The double labelled profiles appear in yellow color.

The study was carried out in ovariectomized female mice grouped into control, vehicle- and clozapine N-oxide (CNO)-treated groups. Serial blood sample (6 minutes) were taken from the tail and their LH content was measured using an ultrasensitive ELISA technique. Blood samples of mice collected before treatment with either vehicle or CNO, showed elevated basal (4.574 ± 1.128 ng/mL and 3.587 ± 1.817 ng/mL) and mean (5.494 ± 2.056 and 6.076 ± 1.237) LH levels. Treatment of mice with CNO significantly increased the mean LH values (9.848 ± 0.985 ng/mL), (**Fig. 11**).

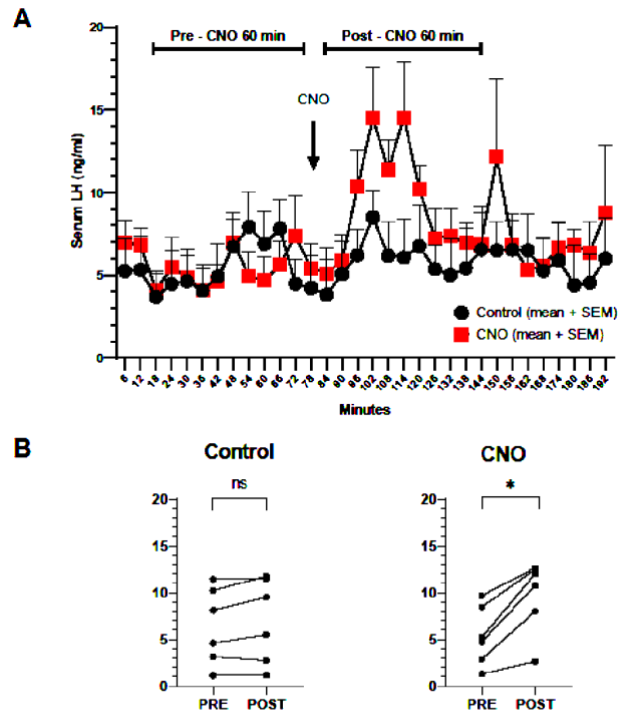


Fig. 11. A. Effect of clozapine N-oxide (CNO) treatment on serum LH level (mean \pm s.e.m) of ovariectomized female mice using an ultrasensitive LH ELISA assay protocol. The frequency of sampling was 6 minutes. The treated (CNO; red squares) and control mice (black dots) received CNO or vehicle, respectively, per os at the 78th minute from the onset of sampling. B) The mean LH serum levels within a 60 minute pre- and post-treatment period were compared in control and CNO- treated mice. While LH levels remained unchanged in the vehicle-treated control group, CNO treatment significantly increased serum LH concentration in the 60-minute post-treatment period (Wilcoxon matched-pairs signed rank test, $p = 0.0313$).

II. Exploration of further novel, central regulators of reproduction

1. Impact of insulin-like growth factor 1 (IGF-1) upon electrophysiology of GnRH neurons

Hypophysiotropic gonadotropin-releasing hormone (GnRH) neurons orchestrate various physiological events that control the onset of puberty. Previous studies showed that insulin-like growth factor 1 (IGF-1) induces the secretion of GnRH and accelerates the onset of puberty, suggesting a regulatory role of this hormone upon GnRH neurons.

To reveal responsiveness of GnRH neurons to IGF-1 and elucidate molecular pathways acting downstream to the IGF-1 receptor (IGF-1R), in vitro electrophysiological experiments were carried out on GnRH-GFP neurons in acute brain slices from prepubertal (23-29 days) and pubertal (50 days) male mice.

Administration of IGF-1 (13 nM) significantly increased the firing rate and frequency of spontaneous postsynaptic currents and that of excitatory GABAergic miniature postsynaptic currents (mPSCs). No GABAergic mPSCs were induced by IGF-1 in the presence of the GABA_A-R blocker picrotoxin. The increase in the mPSC frequency was prevented by the use of the IGF-1R antagonist, JB1 (1 μ M), or the intracellularly applied PI3K blocker (LY294002, 50 μ M), showing involvement of IGF-1R and PI3K in the mechanism. Blockade of the transient receptor potential

vanilloid 1, an element of the tonic retrograde endocannabinoid machinery, by AMG9810 (10 μ M) or antagonizing the cannabinoid receptor type-1 by AM251 (1 μ M) abolished the effect.

These findings indicate that IGF-1 arrests the tonic retrograde endocannabinoid pathway in GnRH neurons, and this disinhibition increases the release of GABA from presynaptic terminals that, in turn, activates GnRH neurons leading to the fine-tuning of the hypothalamo-pituitary-gonadal axis.

2. Effects of gonadal cycle on expression of genes coding for neuropeptide-, growth factor- and orphan GPC-receptors

Rising serum estradiol triggers the surge release of gonadotropin-releasing hormone (GnRH) at late proestrus leading to ovulation. We hypothesized that proestrus evokes alterations in peptidergic signaling onto GnRH neurons inducing a differential expression of neuropeptide-, growth factor-, and orphan G-protein-coupled receptor (GPCR) genes. Thus, we analyzed the transcriptome of GnRH neurons collected from intact, proestrous and metestrous GnRH-green fluorescent protein (GnRH-GFP) transgenic mice using Affymetrix microarray technique. Proestrus resulted in a differential expression of genes coding for peptide/neuropeptide receptors including *Adipor1*, *Prokr1*, *Ednrb*, *Rtn4r*, *Nmbr*, *Acvr2b*, *Sctr*, *Npr3*, *Nmur1*, *Mc3r*, *Cckbr*, and *Amhr2*. In this gene cluster, *Adipor1* mRNA expression was upregulated, and the others were downregulated. Expression of growth factor receptors and their related proteins was also altered showing upregulation of *Fgfr1*, *Igf1r*, *Grb2*, *Grb10*, and *Ngfrap1* and downregulation of *Egfr* and *Tgfr2* genes. *Gpr107*, an orphan GPCR, was upregulated during proestrus, while others were significantly downregulated (*Gpr1*, *Gpr87*, *Gpr18*, *Gpr62*, *Gpr125*, *Gpr183*, *Gpr4*, and *Gpr88*). Further affected receptors included vomeronasal receptors (*Vmn1r172*, *Vmn2r-ps54*, and *Vmn1r148*) and platelet-activating factor receptor (*Ptafr*), all with marked downregulation. Patch-clamp recordings from mouse GnRH-GFP neurons carried out at metestrus confirmed that the differentially expressed IGF-1, secretin, and GPR107 receptors were operational, as their activation by specific ligands evoked an increase in the frequency of miniature postsynaptic currents (mPSCs). These findings show the contribution of certain novel peptides, growth factors, and ligands of orphan GPCRs to regulation of GnRH neurons and their preparation for the surge release.

III. Expanding the biological role of known regulatory peptides of the GnRH system

1. Ghrelin increases food intake via targeting the lateral parabrachial nucleus

The lateral parabrachial nucleus (IPBN) in the brainstem has emerged as a key area involved in feeding control that is targeted by several circulating anorexigenic hormones. Here, the objective was to determine whether the IPBN is also a relevant site for the orexigenic hormone ghrelin, inspired by studies in mice and rats showing that there is an abundance of ghrelin receptors in this area.

This study first explored whether IPBN cells respond to ghrelin involving Fos mapping and electrophysiological studies in rats. Next, rats were injected acutely with ghrelin, a ghrelin receptor antagonist, or vehicle into the IPBN to investigate feeding-linked behaviors.

Curiously, ghrelin injection (intracerebroventricular or intravenous) increased Fos protein expression in the IPBN yet the predominant electrophysiological response was inhibitory. Intra-IPBN ghrelin injection increased chow or high-fat diet intake, whereas the antagonist decreased

chow intake only. In a choice paradigm, intra-IPBN ghrelin increased intake of chow but not lard or sucrose. Intra-IPBN ghrelin did not alter progressive ratio lever pressing for sucrose or conditioned place preference for chocolate.

The IPBN is a novel locus from which ghrelin can alter consummatory behaviors (food intake and choice) but not appetitive behaviors (food reward and motivation).



2. Effects of orexin upon the mesolimbic and mesocortical dopamine projections



Orexin neurons are involved in homeostatic regulatory processes, including arousal, and feeding, and provide a major input from the hypothalamus to the ventral tegmental area (VTA) of the midbrain. VTA neurons are a central hub processing reward and motivation and target the medial prefrontal cortex (mPFC) and the shell part of nucleus accumbens (NAcs). We investigated whether subpopulations of dopamine (DA) neurons in the VTA projecting either to the mPFC or the medial division of shell part of nucleus accumbens (mNAcs) receive differential input from orexin neurons and whether orexin exerts differential electrophysiological effects upon these cells. VTA neurons projecting to the mPFC or the mNAcs were traced retrogradely by Cav2-Cre virus and identified by expression of yellow fluorescent protein (YFP). Immunocytochemical analysis showed that a higher proportion of all orexin-innervated DA neurons projected to the mNAcs (34.5%) than to the mPFC (5.2%). Of all sampled VTA neurons projecting either to the mPFC or mNAcs, the dopaminergic (68.3 vs. 79.6%) and orexin-innervated DA neurons (68.9 vs. 64.4%) represented the major phenotype. Whole-cell current clamp recordings were obtained from fluorescently labelled neurons in slices during baseline periods and bath application of orexin A. Orexin similarly increased the firing rate of VTA dopamine neurons projecting to mNAcs (1.99 ± 0.61 Hz to 2.53 ± 0.72 Hz) and mPFC (0.40 ± 0.22 Hz to 1.45 ± 0.56 Hz). Thus, the hypothalamic orexin system targets mNAcs and to a lesser extent mPFC-projecting dopaminergic neurons of the VTA and exerts facilitatory effects on both clusters of dopamine neurons.

IV. Scientometric data of papers published with NKFIH support

Number of papers	7
Cumulative impact value	29,566

V. List of relevant publications

[Kalló, Imre](#) ; [Omrani, Azar](#) ; [Meye, Frank J.](#) ; [de Jong, Han](#) ; [Liposits, Zsolt](#)  ; [Adan, Roger A. H.](#) 
[*Characterization of orexin input to dopamine neurons of the ventral tegmental area projecting to the medial prefrontal cortex and shell of nucleus accumbens*](#)
 BRAIN STRUCTURE & FUNCTION 227: 3 pp. 1083-1098., 16 p. (2022)
[DOI WoS](#) [REAL](#) [Scopus](#)

[Balint, Flora](#) ; [Csillag, Veronika](#) ; [Vastagh, Csaba](#) ; [Liposits, Zsolt](#)  ; [Farkas, Imre](#) 
[*Insulin-like growth factor 1 \(IGF-1\) increases GABAergic neurotransmission to GnRH neurons via suppressing the retrograde tonic endocannabinoid signaling pathway in mice.*](#)
 NEUROENDOCRINOLOGY 111: 12 pp. 1219-1230. , 12 p. (2021)
[DOI WoS](#) [REAL](#) [Scopus](#) [PubMed](#)

[Vastagh, Csaba](#) ; [Farkas, Imre*](#) ; Scott, Michael M ; [Liposits, Zsolt](#) ✉
[Networking of glucagon-like peptide-1 axons with GnRH neurons in the basal forebrain of male mice revealed by 3DISCO-based immunocytochemistry and optogenetics.](#)
BRAIN STRUCTURE & FUNCTION 226: 1 pp. 105-120. , 16 p. (2021)
[DOI WoS](#) [REAL](#) [Scopus](#) [PubMed](#)

[Vastagh, Csaba](#) ; [Csillag, Veronika](#) ; Solymosi, Norbert ; [Farkas, Imre](#) ; [Liposits, Zsolt](#) ✉
[Gonadal Cycle-Dependent Expression of Genes Encoding Peptide-, Growth Factor-, and Orphan G-Protein-Coupled Receptors in Gonadotropin- Releasing Hormone Neurons of Mice](#)
FRONTIERS IN MOLECULAR NEUROSCIENCE 13 Paper: 594119, 17 p. (2021)
[DOI WoS](#) [REAL](#) [Scopus](#)

Bake, Tina ; Le May, Marie V. ; Edvardsson, Christian E. ; Vogel, Heike ; Bergström, Ulrika ; Albers, Marjorie Nicholson ; Skibicka, Karolina P. ; [Farkas, Imre](#) ; [Liposits, Zsolt](#) ; Dickson, Suzanne L. ✉
[Ghrelin Receptor Stimulation of the Lateral Parabrachial Nucleus in Rats Increases Food Intake but not Food Motivation](#)
OBESITY 28: 8 pp. 1503-1511. , 9 p. (2020)
[DOI WoS](#) [REAL](#) [Scopus](#)

[Csillag, Veronika](#) ; [Vastagh, Csaba](#) ; [Liposits, Zsolt](#) ; [Farkas, Imre](#) ✉
[Secretin Regulates Excitatory GABAergic Neurotransmission to GnRH Neurons via Retrograde NO Signaling Pathway in Mice.](#)
FRONTIERS IN CELLULAR NEUROSCIENCE 13 Paper: 371, 14 p. (2019)
[DOI WoS](#) [REAL](#) [Scopus](#) [PubMed](#)

[Vastagh, Csaba](#) ; [Solymosi, Norbert](#) ; [Farkas, Imre](#) ; [Liposits, Zsolt](#) ✉
[Proestrus Differentially Regulates Expression of Ion Channel and Calcium Homeostasis Genes in GnRH Neurons of Mice](#)
FRONTIERS IN MOLECULAR NEUROSCIENCE 12 Paper: 137, 14 p. (2019)
[DOI WoS](#) [REAL](#) [Scopus](#)